Vision and Motion Planning for a Mobile Robot under Uncertainty

Jun Miura

Yoshiaki Shirai

Department of Computer-Controlled Mechanical Systems

Osaka University

Suita, Osaka 565-0871, Japan
jun@mech.eng.osaka-u.ac.jp

Abstract

This paper describes a framework for vision and motion planning for a mobile robot. The task of the robot is to reach the destination in the minimum time while it detects possible routes by vision. Since visual recognition is computationally expensive and the recognition result includes uncertainty, a trade-off must be considered between the cost of visual recognition and the effect of information to be obtained by recognition. Using a probabilistic model of the uncertainty of the recognition result, vision-motion planning is formulated as a recurrence formula. With this formulation, the optimal sequence of observation points is recursively determined. A generated plan is globally optimal because the planner minimizes the total cost. An efficient solution strategy is also described which employs a pruning method based on the lower bound of the total cost calculated by assuming perfect sensor information. Simulation results and experiments with an actual mobile robot demonstrate the feasibility of our approach.

1 Introduction

There has been an increasing interest in autonomous mobile robot which recognizes an environment with vision and moves without guidance of human operators. A key to realize such a robot is the ability to generate a plan of vision and motion operations so that a robot can efficiently reach the destination. To design a planning algorithm for such a robot, we need to consider two characteristics of visual recognition: *cost* and *uncertainty*. Visual recognition is generally costly because the image data is large, and because relatively complicated reasoning is necessary. Visual information contains uncertainty from many sources such as discretization.

This paper is concerned with vision-motion planning for a mobile robot navigation in a *known* but *uncertain* indoor environment. We consider situations where there are only known objects and their rough positions are also known. Such a situation arises, for example, in a typical office environment; the position of desks, chairs, and other furniture are roughly known, while their exact positions are uncertain; some chairs may block the robot from taking a certain path to the destination.

In such a situation, a robot has to determine the location of objects and the passable space between objects so that it can maneuver about the objects. Fig. 1 illustrates a typical example of such a situation. The objective of planning here is to generate a *sequence* of observation points and observation conditions which leads the robot to the goal point at the minimum cost (in the minimum time). Only the passability of each space is uncertain, which the robot determines by vision.
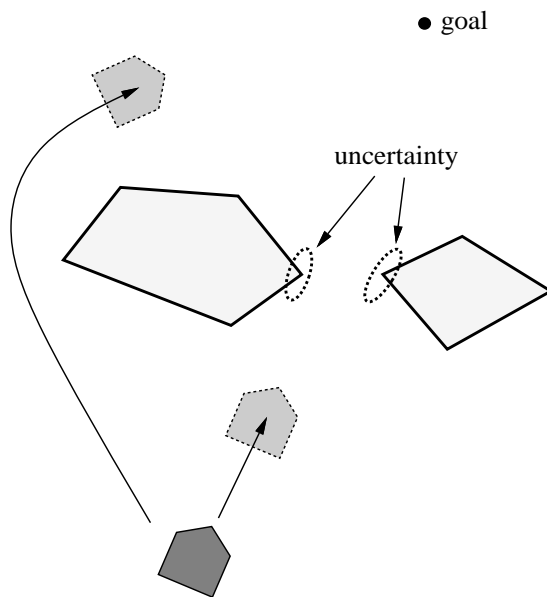
Figure 1: A sample situation.

Let us consider two behaviors of the robot in Fig. 1: one is to approach the objects and to observe the objects again in order to obtain more accurate information for further planning; the other is to take a known detour immediately without further observations. To decide which behavior is better, we first need to consider not only the cost of motion but also that of visual recognition. Moreover, for determining the best observation points for the former behavior,

it is necessary to consider a trade-off between the cost of visual recognition and the effect of information to be obtained.

Decision theory is a useful tool to evaluate such trade-offs. If the information used for decision making is uncertain, and some statistical knowledge of the uncertainty is available, statistical decision theory can be very useful.

Feldman and Sproull (1977) first applied decision theory to planning, where a success ratio of each motion and a utility function for the comparison of plans were given in advance.

Hu and Brady (1994) applied Bayesian decision theory to on-line path selection of a mobile robot. The proposed method dealt with selection of a single-step action based on the current information, and the resultant behavior is not always globally optimal.

Cameron and Durrant-Whyte (1990) applied Bayesian decision theory to optimal sensor placement. A utility function was given which represents a kind of accuracy of information. Hutchinson and Kak (1989) used Dempster-Shafer theory to represent uncertainties of hypotheses in object identification. The entropy of a hypothesis set was used as a utility function and a sensor placement was selected which minimizes the entropy. Zheng (1992) proposed a similar method. These works did not consider the cost of sensing.

Hager (1990) described a decision-theoretic approach to sensor planning, in which the cost of sensing is considered. In this approach, each task requires a new utility function which evaluate the effect of a sensing action. He also considered a planning for multiple actions, and employed a fixed sample size n-step look ahead approximation (1985) to increase the quality of the resultant plan. Dean et al. (1990) proposed to use a network of probabilistic dependency to cope with similar planning problems. Similar to the above work, a plan was evaluated based on a predetermined utility function with limited look ahead. In these approaches, a utility function tries to evaluate how each action (or a short sequence of actions) is appropriate for optimizing the whole behavior. Such a utility function needs to be designed for each task, sometimes in a heuristic manner. In addition, since a whole plan is not evaluated at once, the resultant behavior is not always globally optimal.

In this paper, we propose to evaluate the utility of a sequence of sensing actions by evaluating the efficiency of a whole plan, i.e., the total execution cost of the plan. This utility measure is general and appropriate for almost all tasks, and the selected plan is globally optimal. This approach, however, should be accompanied with efficient search strategies to cope with combinatorial explosion which is caused by a long lookahead.

This paper formulates a vision-motion planning for a mobile robot with stereo vision along the above-mentioned approach. The cost of visual recognition is considered as well as that of motion. Uncertainty of recognition results are represented by a probabilistic model. A plan is selected which minimizes the expectation of the total cost for accomplishing a given task. By predicting recognition results using the model of uncertainty, the planner recursively searches for an optimal sequence of observation points by the branch-and-bound method. An efficient pruning method is developed which is based on the lower bound of the total cost calculated by the *assumption of perfect sensor information*.

In this paper, we assume the motion estimation of the mobile robot is fairly accurate, and therefore the motion uncertainty is negligible. It is possible, however, to cope with the case of large motion uncertainty by combining the motion uncertainty with the vision uncertainty and making a plan for the combined uncertainty.

The rest of this paper is organized as follows. Section 2 describes our formulation of vision-motion planning, which is basically represented by a recurrence formula. A search strategy using the branch-and-bound method is also described. Section 3 describes an uncertainty model of

stereo vision. Section 4 describes a method of predicting sensor information based on fusion of predicted sensor data. Section 5 describes how to calculate the lower bound of alternative actions using the probabilistic uncertainty model of visual information. Section 6 describes simulation results, preceded by some implementation issues. Section 7 describes experimental results for actual planning problems. Section 8 summarizes the paper and describes future works.

2 Formulation of Vision-Motion Planning Problem

2.1 Formulation in a Recurrence Formula

This section describes a general formulation of a vision-motion planning problem with uncertainty. We assume that information about the environment is represented by a multivariate probabilistic distribution, each variable of which is a property of the environment such as the position of a feature, and that an observation result is represented by a vector of such properties with uncertainties, which is also represented by a multivariate probabilistic distribution.
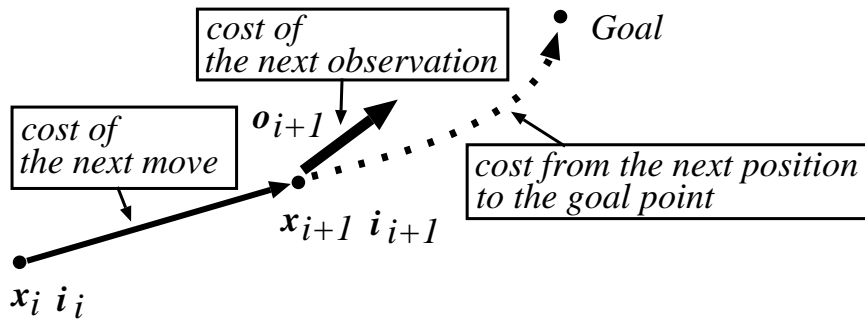
Figure 2: Calculating the cost to the goal point.

The quality of a plan is evaluated by its execution cost. Since a plan is generated based on probabilistic information, the planner selects a sequence of observation points so that the expectation of the total cost for reaching the destination is minimized. We here derive a recurrence formula which calculates the optimal next observation point x_{i+1} and the optimal next observation condition O_{i+1}, such as the observation direction, from the current observation point x_i and the current information I_i. As indicated in Fig. 2, for the robot at x_i with information I_i, the cost to the destination is given by the sum of the following three costs:

1. the cost of motion to the next observation point,

2. the cost of the next observation,

3. the cost from the next observation point to the destination.

The next observation point and condition (x_{i+1} and O_{i+1}) are determined so that the sum is minimized. Since the optimal plan after the next observation depends on the observation result, in the minimization process, the expectation of the minimum cost is used for the third term. Thus, the following recurrence formula is derived:
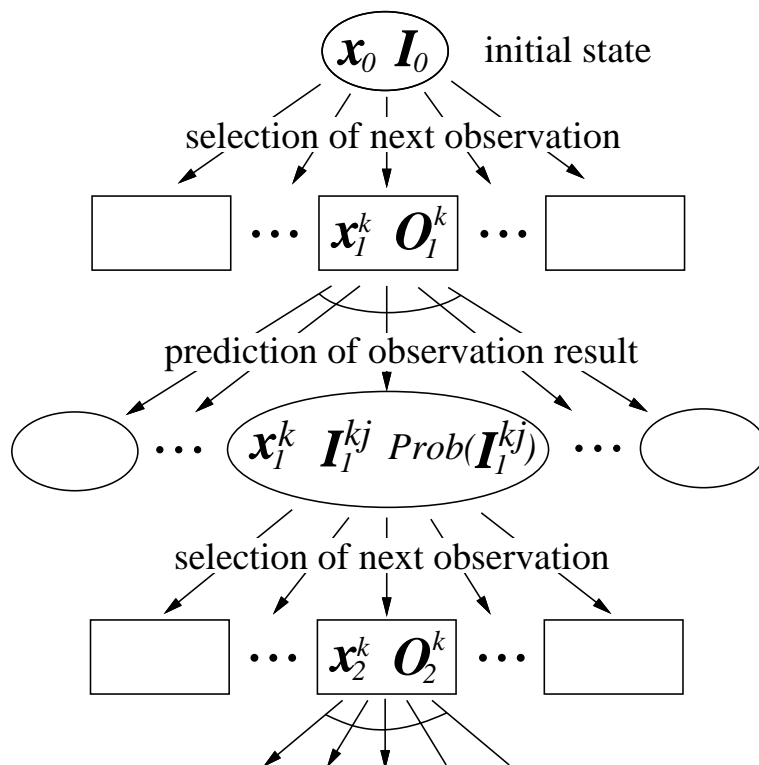
Figure 3: An AND/OR search tree.
Rectangles indicate OR nodes; Ellipses indicate AND nodes.

$$C_{optimal}(\boldsymbol{x}_i, \boldsymbol{I}_i) = \min_{\substack{\boldsymbol{x}_{i+1} \in \mathcal{X} \\ \boldsymbol{O}_{i+1} \in \mathcal{O}}} \left(\begin{array}{c} C_{motion}(\boldsymbol{x}_i, \boldsymbol{x}_{i+1}) + C_{vision}(\boldsymbol{O}_{i+1}) + \\ \int Prob(\boldsymbol{I}_{i+1}) C_{optimal}(\boldsymbol{x}_{i+1}, \boldsymbol{I}_{i+1}) d\boldsymbol{I}_{i+1} \end{array} \right). \tag{1}$$

$C_{optimal}(\boldsymbol{x}, \boldsymbol{I})$: The optimal cost with information $\boldsymbol{I}$ at $\boldsymbol{x}$.
$C_{motion}(\boldsymbol{x}, \boldsymbol{y})$: The cost of motion from $\boldsymbol{x}$ to $\boldsymbol{y}$.
$C_{vision}(\boldsymbol{O})$: The cost of observation $\boldsymbol{O}$.
$Prob(\boldsymbol{I})$: The probability of acquiring information $\boldsymbol{I}$.
$\mathcal{X}$: A possible range of $\boldsymbol{x}_{i+1}$.
$\mathcal{O}$: A possible range of $\boldsymbol{O}_{i+1}$.

If there are direct paths to the destination which a robot can follow without examining the passability of any space (we call such paths *direct-path solutions*), the optimal (minimum-cost) direct path solution is selected and compared with the solution of Equation (1), and finally the better one is selected.

In order to solve Equation (1), the planner recursively searches for an optimal sequence of observation points. The search tree becomes an AND/OR tree (see Fig. 3); an OR node corresponds to an observation condition at an observation point; an AND node corresponds to possible information after an observation (see Section 4). By selecting an observation position and an observation condition (OR node), each predicted information after the observation (AND node) is automatically calculated. A solution is also an AND/OR tree because the actual behavior of the robot after an observation depends on the observation result.

2.2 Termination Condition

Since every observation result includes uncertainty, the resultant observed data always include uncertainty and never converges to deterministic values. This fact may lead one to believe that the above-mentioned recursive computation never terminates. In terms of passability, however, situations can become deterministic. Let us consider the situation shown in Fig. 1. Suppose the robot has obtained a probability distribution of the distance between the objects. According to the relationship between the distribution and the robot width, possible situations can be classified into three cases (Fig. 4): if the lower bound of the distribution is larger than the robot width (case (a)), the space between the objects is passable; if the upper bound of the distribution is smaller than the robot width (case (b)), the space is impassable; otherwise (case (c)), the robot cannot decide the passability of the space. In the first two cases, the situation is now deterministic in terms of passability, and no further sensing is necessary for this space.
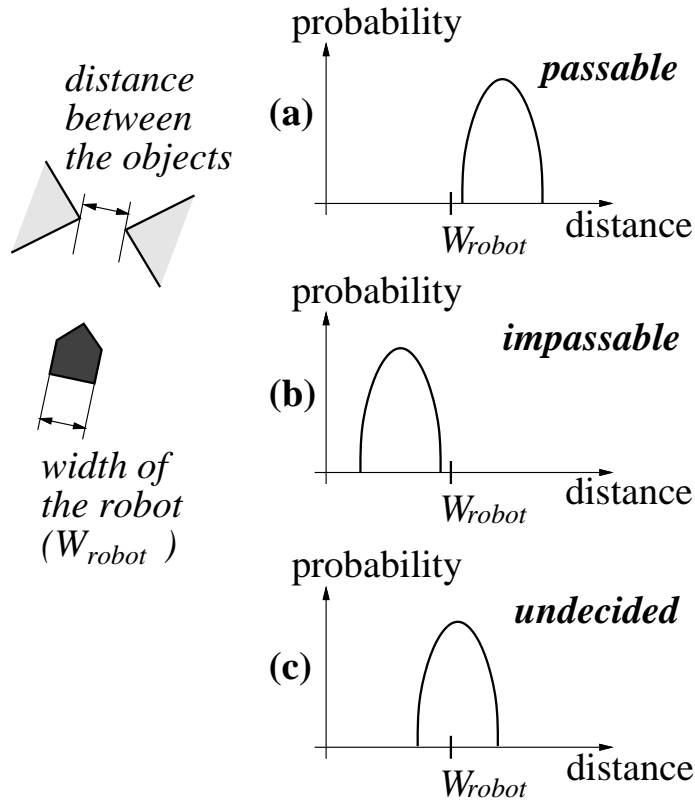
Figure 4: Three possible relations between the robot width and the distribution of the distance between objects.

2.3 Search with Branch-and-Bound

In our formulation, the cost for solving a vision-motion planning problem is roughly given by $\mathcal{O}((mnl)^k)$; m is the average number of observation points; n is the average number of observation conditions; l is the average number of possible observation results; and k is the average depth of the search tree. An exhaustive search at each level of the search tree may cause

combinatorial explosion. Among the above parameters which specify the computational cost, m and n are reducible by employing a pruning method; others depend on the problem setting. In this paper, we employ the branch-and-bound method with best-bound search (Ibaraki 1987) to obtain the optimal solution efficiently.

Under the planning process, there are many candidates for the solution. Each candidate is an AND/OR tree whose leaves are either open OR nodes or deterministic nodes; a deterministic node is the node for which the final (deterministic) action is assigned (see Fig. 5). Each candidate, in general, has multiple open nodes. Although every open node can be expanded next, the open node which has the highest probability is to be expanded next in order to reduce the search cost.

initial state

AND node (open)
AND node (expanded) } state
OR node (non–deterministic) } selected
OR node (deterministic) } action
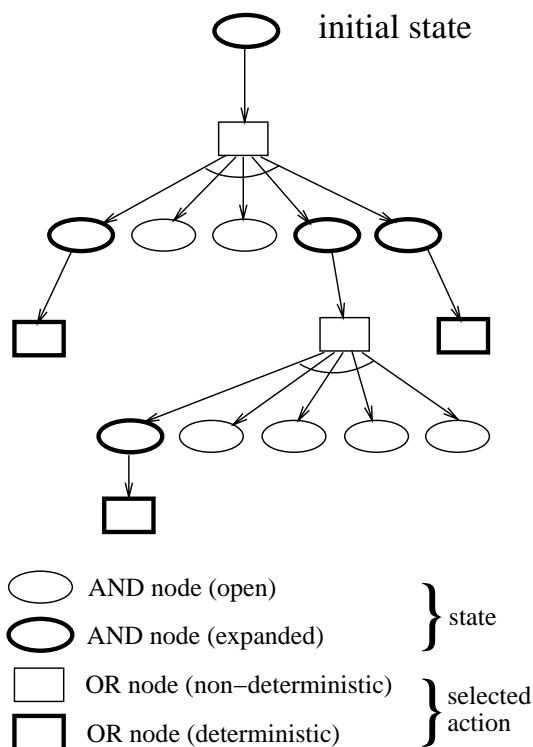
Figure 5: A candidate of solution is a partially expanded AND/OR tree.

There is a list which contains solution candidates (or solutions) in ascending order of the lower bound (or the actual value) of the cost. In the search process, the head of the list is picked up and expanded iteratively. When an OR node of a solution candidate is expanded, the lower bounds or the deterministic actions for its successive open OR nodes are calculated, and the modified candidate is put into the list. If the head of the list is a solution, it is the optimal one, and the search terminates. The planner also keeps the incumbent, i.e., the best feasible solution among those which have been acquired so far (Ibaraki 1987). If the lower bound of the cost of a candidate is larger than the cost of the incumbent, the candidate is eliminated because the candidate can never produce a better solution than the incumbent.

The quality of the lower bound affects the efficiency of the search process, that is, the nearer the lower bound of the cost of a solution candidate is to the actual cost, the more efficiently the optimal solution is found. Section 5 will discuss a method of calculating the lower bound

using the uncertainty model of vision.

2.4   Use of Easily-Obtainable Feasible Solutions

By employing the best-bound search, the number of expanded nodes is minimized. A large number of unresolved candidates (candidates containing open OR nodes), however, must be kept in memory during search. A feasible solution can be used as an incumbent to eliminate useless candidates, and thereby to reduce the memory space. Thus, if a good feasible solution is easily obtained, it is worth calculating.

We currently use one type of feasible solution. In the feasible solution, a robot observes each space at most once. If a space is decided to be passable, the robot may use the space; otherwise, the space is not used.

If the passability of each space is low, the feasible solution is especially useful. This fact is explained as follows. Since only for the unknown case, further observations are searched for in order to obtain the optimal solution, if that probability is small, the difference between the cost of the feasible solution and that of the optimal one becomes small.

If there are multiple spaces to be observed, the best order of observing each space is calculated, and one feasible solution is generated. At the beginning of the expansion of an OR node, we calculate this feasible solution for the node. If the new feasible solution is less costly than the current incumbent, the new solution becomes the incumbent. The feasible solution for the initial state is used as the initial incumbent.

In time-bounded situations, a feasible solution may be used as the solution to the problem. When the planning time is exhausted, the current incumbent may be returned as the final solution.

3   Uncertainty Modeling of Stereo Vision

This section describes the uncertainty modeling of a segment-based stereo vision. There are various sources of uncertainty such as quantization error in images (Matthies and Shafer 1987; Ayache and Faugeras 1989; Kriegman, Triendl, and Binford 1989), calibration errors (Ayache and Faugeras 1989) and stereo matching ambiguity (Miura and Shirai 1993).

The uncertainty caused by quantization error is modeled using a normal distribution, as explained in Section 3.2. This modeling is verified using actual data in Section 7.1. Calibration errors are also reasonably modeled using normal distributions as long as they are unbiased. In this paper, therefore, we construct the uncertainty model by considering only quantization error because calibration errors can approximately be included in this model, if necessary, by adjusting its covariance matrix.

3.1   Segment-Based Stereo Vision

In indoor scenes, there are many line segments that are components of artificial objects. Such segments are useful as primitive features for stereo matching because structural information is implicitly imposed as constraints (Medioni and Nevatia 1985). Especially, vertical line segments are useful for a mobile robot to detect collision-free areas on the floor. Thus, we use only vertical segments and consider their two-dimensional position on the floor.

We here treat a stereo system (Miura and Shirai 1993) in which two cameras are mounted in parallel with each other and with the floor. Thus, vertical segments in a real scene are

projected as vertical segments onto the image plane. For a pair of matched segments, the horizontal position of each segment is calculated by fitting a line to the overlapping part of the segment (see Fig. 6). The position of the segment in a real scene is then calculated by triangulation.
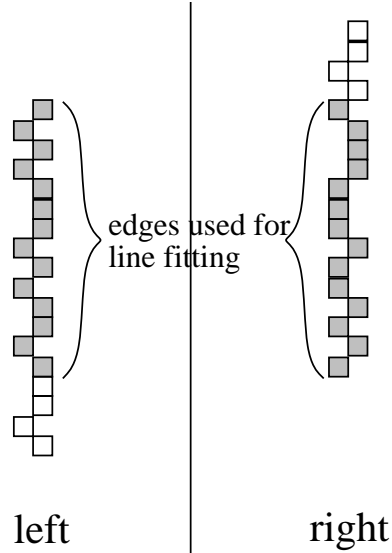
Figure 6: Valid parts of segments.

3.2   Model of Uncertainty Caused by Quantization Error

The uncertainty of an edge's horizontal position caused by quantization error is modeled by a uniform distribution of one-pixel wide. Since the horizontal position of a vertical segment in the image is calculated as the mean position of its edges, and since the distribution of each edge position is considered to be independent, the distribution of the segment position can be approximated by a normal distribution (*the central limit theorem* (Fisz 1963)). In addition, that distribution is apparently bounded within the range of one pixel. Thus, we use a certain part of the normal distribution.

We then derive the positional uncertainty of a segment in a real scene. Suppose a vertical line segment at (x, z) is projected onto the right and the left image at X_l and X_r, respectively (see Fig. 7). The following equation is derived:

$$\begin{pmatrix} x \\ z \end{pmatrix} = \frac{1}{X_l - X_r} \begin{pmatrix} a(X_l + X_r) \\ 2af \end{pmatrix},$$

where $2a$ is the baseline and f is the focal length of the cameras.

Since the uncertainties of both segments are independent, and since the effective numbers of edges are the same for both segments (see Fig. 6), the distribution of a vector (X_l, X_r) becomes a two-dimensional normal distribution; its covariance matrix $\Lambda_{(X_l, X_r)}$ is given by

$$\Lambda_{(X_l, X_r)} = \begin{pmatrix} \sigma_{img}^2 & 0 \\ 0 & \sigma_{img}^2 \end{pmatrix},$$

9
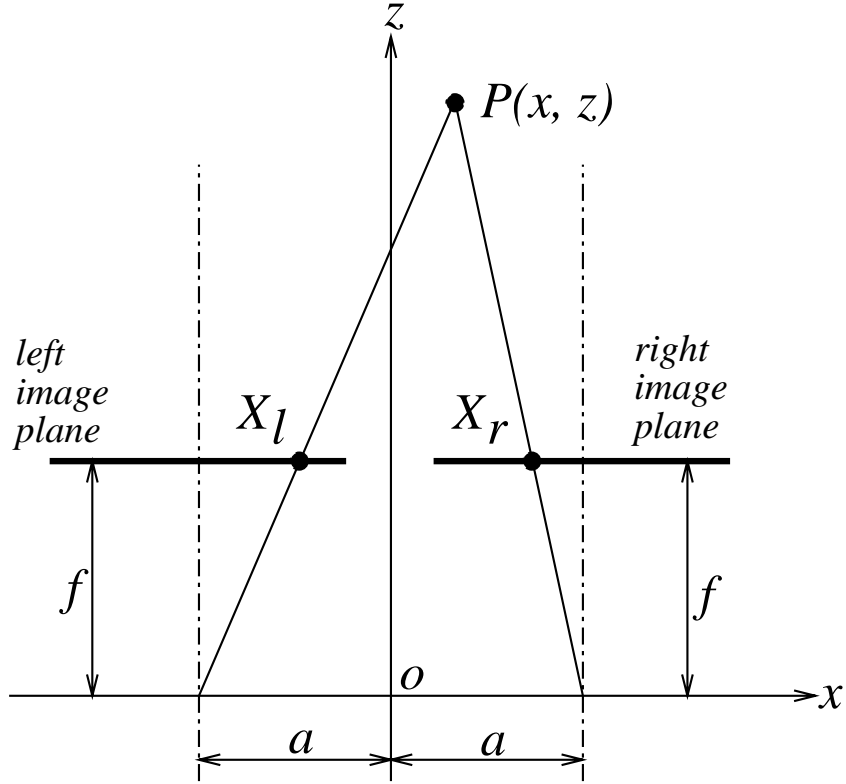
Figure 7: Geometry of a stereo system.

where σ_{img}^2 is the variance of the distribution of the horizontal position of each segment in the image. The value of σ_{img}^2 is approximately inversely proportional to the number of edges in a segment (Fisz 1963).

Assuming that σ_{img} is small enough compared with $X_l - X_r$, by linearizing the equation of image projection using up to the first order terms of Taylor expansion, the position of a segment in a real space is represented by a two-dimensional normal distribution (Kriegman, Triendl, and Binford 1989; Matthies and Shafer 1987). Letting (μ_l, μ_r) be the mean vector of the distribution of (X_l, X_r), the linearized equation is given by

$$
\begin{pmatrix} x \\ z \end{pmatrix} = A \begin{pmatrix} X_l \\ X_r \end{pmatrix} + \boldsymbol{b},
$$

$$
A = \frac{2a}{(\mu_l - \mu_r)^2} \begin{pmatrix} -\mu_r & \mu_l \\ -f & f \end{pmatrix},
$$

$$
\boldsymbol{b} = \frac{a}{\mu_l - \mu_r} \begin{pmatrix} \mu_l + \mu_r \\ 4f \end{pmatrix}.
$$

Thus, the covariance matrix $\Lambda_{(x,z)}$ of the distribution of (x,z) is given by

$$
\Lambda_{(x,z)} = A\Lambda_{(X_l,X_r)}A^T,
$$

where T indicates transpose.

3.3 Uncertainty of the Width of a Space

Using the above model of uncertainty, we can compute the uncertainty of the width of a space which a robot may pass through. Suppose that a robot is measuring the distance between two features at $\boldsymbol{x}_l$ and $\boldsymbol{x}_r$ (see Fig. 8). Let $P_l(\boldsymbol{x}_l)$ and $P_r(\boldsymbol{x}_r)$ denote their positional distributions. From the above-mentioned uncertainty model of stereo vision, $P_l(\boldsymbol{x}_l)$ and $P_r(\boldsymbol{x}_r)$ are normal distributions; let $\boldsymbol{\mu}_l$, $\boldsymbol{\mu}_r$, Σ_l, and Σ_r be the means and the covariance matrices of them, respectively.

The distribution $P(d)$ of the distance d is given by

$$P(d) = \int \int_{\|\boldsymbol{x}_l - \boldsymbol{x}_r\| = w} P_l(\boldsymbol{x}_l) P_r(\boldsymbol{x}_r) d\boldsymbol{x}_l d\boldsymbol{x}_r. \tag{2}$$

Since the equation $d = \| \boldsymbol{x}_l - \boldsymbol{x}_r \|$ is non-linear, the distribution $P(d)$ is not normally distributed. Allen et al. (1991) derived a closed form using a modified Bessel function in case that the distribution of $\boldsymbol{x}_l - \boldsymbol{x}_r$ is a two-dimensional normal distribution, and that the distribution is isotropic, i.e., the equi-probability contour of the distribution is a circle. In general, however, we cannot obtain the closed form of the probability density function of d. Thus, we approximate the distribution of d by a one-dimensional normal distribution by assuming that $\|\Delta\boldsymbol{x}_l\|$ and $\|\Delta\boldsymbol{x}_r\|$ are considered to be small enough as compared with $\| \boldsymbol{\mu}_l - \boldsymbol{\mu}_r \|$.

Using up to the first order terms of Taylor expansion of Equation (2), we obtain

$$d = \| \boldsymbol{\mu}_l - \boldsymbol{\mu}_r \| + J_l(\boldsymbol{x}_l - \boldsymbol{\mu}_l) + J_r(\boldsymbol{x}_r - \boldsymbol{\mu}_r),$$

where J_l (J_r) is the Jacobian matrix from $\Delta\boldsymbol{x}_l$ ($\Delta\boldsymbol{x}_r$) to Δd at $(\boldsymbol{\mu}_l, \boldsymbol{\mu}_r)$. The mean μ_d and the variance σ_d^2 of the distance between the points is given by

$$\mu_d \;\; = \;\; \| \boldsymbol{\mu}_l - \boldsymbol{\mu}_r \| \tag{3}$$
$$\sigma_d^2 \;\; = \;\; J_l \Sigma_l J_l^T + J_r \Sigma_r J_r^T. \tag{4}$$

Note that the positional distributions for the left segment and the right one are independent of each other.

Fig. 9 shows the change of the variance of the distance (σ_d^2) according to the change of the observation point. From the figure, we can see that the variance depends not only on the observation distance but also on the observation direction. For the case of Fig. 9, we calculated the actual mean and variance from Equation (2) by numerical integration and compared the actual values with the approximate ones in terms of error ratios. The maximum and the average error ratio with respect to the actual values are 0.12% and 0.02% for the mean, and 5.63% and 2.98% for the variance, respectively. This result shows that the approximation is reasonable. This approximation will also be verified using actual data in Section 7.1.

Since the positional distribution of vertical segments are bounded as mentioned above, the distribution of the width of a space is also bounded; we use the $\pm 3\sigma$ points as boundaries.

4 Prediction of Sensor Information

To make a plan including sensing, a robot must be able to predict sensor information. More concretely, we need to calculate the information after an observation, which is indicated as $\boldsymbol{I}_{i+1}$ in Equation (1), to solve a problem. This section explains how to predict sensor information.
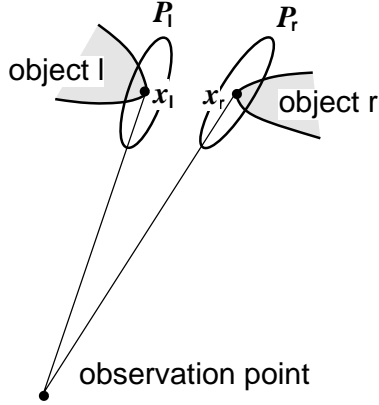
Figure 8: Distributions of two feature positions.
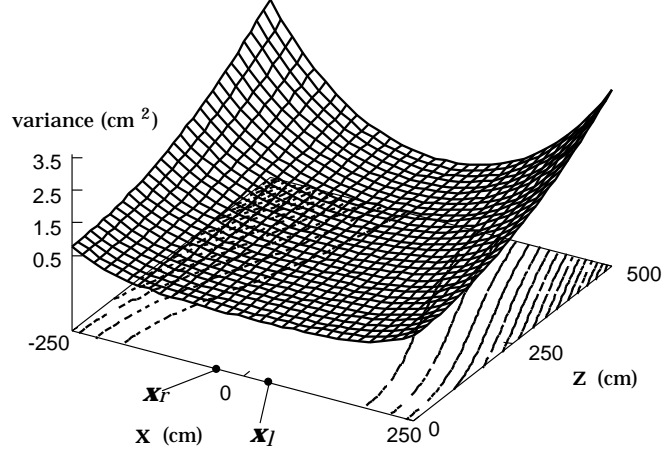
Figure 9: Change of the variance of the distance using an approximate normal distribution. The means of feature positions are $(-40, 0)$ and $(40, 0)$.

4.1 Predicting Information after an Observation

Suppose that a robot is estimating a scalar property x such as the width of a space, and that the uncertainty of information is represented by a normal distribution. Let a normal distribution $N(\mu_0, \sigma_0^2)$ be the current distribution of the scalar property acquired by the sensing so far. Assume the uncertainty σ_{obs}^2 of the next observation result is constant regardless of the true value x_{true} of x.

If the next observation result is x_{obs}, we can consider that the newly obtained information is $N(x_{obs}, \sigma_{obs}^2)$. Thus, using Bayes' theorem, the information after the next observation is given by $N(\mu_1, \sigma_1^2)$, where

$$\mu_1 \;=\; \frac{\sigma_{obs}^2 \mu_0 + \sigma_0^2 x_{obs}}{\sigma_0^2 + \sigma_{obs}^2} \quad \text{and} \tag{5}$$

$$\sigma_1^2 \;=\; \frac{\sigma_0^2 \sigma_{obs}^2}{\sigma_0^2 + \sigma_{obs}^2}. \tag{6}$$

In actual, we cannot know in advance the actual value of x_{obs}. Instead, we can predict the distribution of x_{obs} from the current information $N(\mu_0, \sigma_0^2)$ and the uncertainty σ_{obs}^2 in the next observation result. The distribution $P(x_{obs})$ is calculated as follows:

$$
\begin{aligned}
P(x_{obs}) \;&=\; \int_{-\infty}^{\infty} P(x_{obs}|x_{true})P(x_{true})dx_{true} \\
&=\; \int_{-\infty}^{\infty} \frac{1}{\sqrt{2\pi\sigma_{obs}^2}} e^{-(x_{obs}-x_{true})^2/2\sigma_{obs}^2} \cdot \frac{1}{\sqrt{2\pi\sigma_0^2}} e^{-(x_{true}-\mu_0)^2/2\sigma_0^2} dx_{true} \\
&=\; \frac{1}{\sqrt{2\pi(\sigma_0^2+\sigma_{obs}^2)}} e^{-(x_{obs}-\mu_0)^2/2(\sigma_0^2+\sigma_{obs}^2)}.
\end{aligned}
\tag{7}
$$

Once the distribution of x_{obs} is calculated, we can obtain a set of possible distributions and their probabilities after the next observation. As shown in Fig. 10, for each possible value
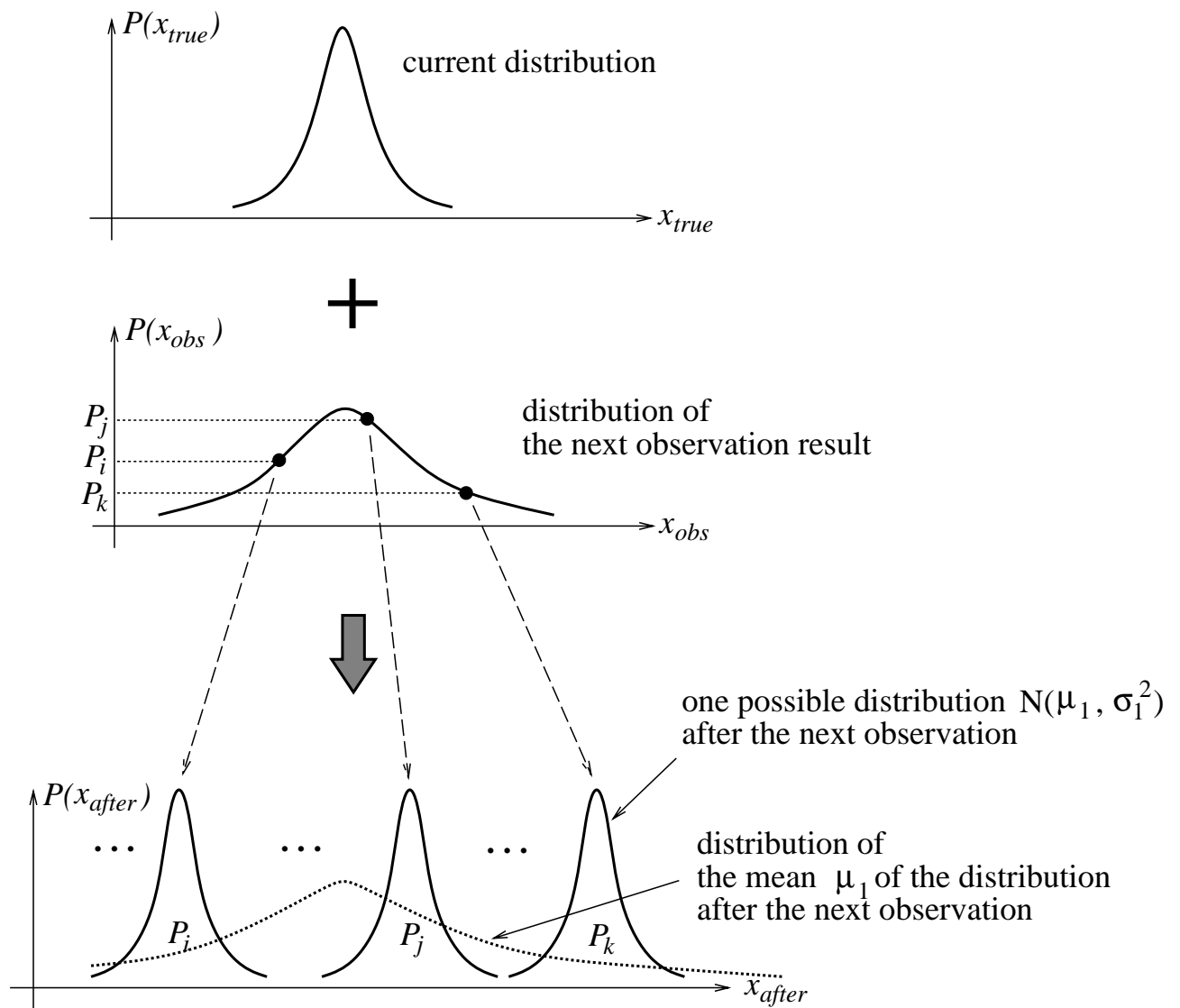
Figure 10: Prediction of information after an observation with uncertainty. For each possible observation result x_{obs}, the distribution $N(\mu_1, \sigma_1^2)$ after the next observation is calculated. As a result, a set of possible distributions is obtained. The probability of obtaining each possible distribution is equal to the probability of the corresponding observation result.

of x_{obs}, the distribution after observation is calculated; its variance, given by Equation (6), is constant; its mean, given by Equation (5), varies depending on the observation result x_{obs}.

Let us derive the *distribution* of the mean μ_1 of the distribution after observation. In general, if two variables p and q have a linear relation $q = ap + b$, and if the distribution of p is $N(\mu, \sigma^2)$, q is also normally distributed with $N(a\mu + b, (a\sigma)^2)$. Since μ_1 is linear to x_{obs} from Equation (5), and since the distribution of x_{obs} is $N(\mu_0, \sigma_0^2 + \sigma_{obs}^2)$ from Equation (7), μ_1 is normally distributed. The mean of the distribution of μ_1 is given by

$$\frac{\sigma_{obs}^2 \mu_0 + \sigma_0^2 \mu_0}{\sigma_0^2 + \sigma_{obs}^2} = \mu_0, \tag{8}$$

and the variance $\sigma_{\mu_1}^2$ is given by

$$\sigma_{\mu_1}^2 = \left(\frac{\sigma_0^2}{\sigma_0^2 + \sigma_{obs}^2}\right)^2 (\sigma_0^2 + \sigma_{obs}^2) = \frac{\sigma_0^4}{\sigma_0^2 + \sigma_{obs}^2}. \tag{9}$$

To summarize, the distribution after the next observation is given by Equations (5) and (6); especially, $N(\mu_0, \sigma_0^4/(\sigma_0^2 + \sigma_{obs}^2))$ specifies the distribution of μ_1.[1]

Note that even if the motion uncertainty is not negligible, the observed width of a space is not affected by the uncertainty because the width is calculated as the relative distance between two segments in a single pair of stereo images.

4.2 Predicting the Passability of a Space

Let us consider the problem of predicting the passability of a space. After the next observation, the robot classifies the state of the space into one of the following three states: (1) the space is passable; (2) the space is impassable; (3) the passability is still unknown. Because the classification result depends on information after the next observation, the robot cannot know the result in advance. The robot, however, *can* predict the the probabilities of the three states without obtaining actual data. These probabilities, which we denote as $P_\bigcirc$, $P_\times$, and $P_\triangle$ for the passable, impassable, and unknown cases, respectively, are calculated as follows.

We use the uncertainty model of stereo vision described in the previous section; the uncertainty of the width of the space is modeled with a certain portion (i.e., within $\pm 3\sigma$ points) of a normal distribution. In this case, the criterion on passability, which is shown in Fig. 4 in Section 2.2, is stated as follows. If the robot width (W_{robot}) is outside the boundaries ($\pm 3\sigma$ points), the situation is deterministically passable or impassable; otherwise, the passability is unknown.

---

[1]This fact is verified by calculating the distribution of the width of the space assuming that every possible x_{obs} is observed with probability indicated by $N(\mu_0, \sigma_0^2 + \sigma_{obs}^2)$. This calculation is done by the following integration:

$$\int_{-\infty}^{\infty} \frac{1}{\sqrt{2\pi(\sigma_0^2 + \sigma_{obs}^2)}} e^{-(x_{obs} - \mu_0)/2(\sigma_0^2 + \sigma_{obs}^2)} \cdot \frac{1}{\sqrt{2\pi\sigma_1^2}} e^{-(x - \mu_1)/2\pi\sigma_1^2} dx_{obs}.$$

The result of the integration becomes

$$\frac{1}{\sqrt{2\pi\sigma_0^2}} e^{-(x - \mu_0)/2\sigma_0^2}.$$

This is the original distribution before observation because no information has been added in actual.

Following the notation above, let $N(\mu_0, \sigma_0^2)$ be the current distribution of the width of the space, and σ_{obs}^2 be the uncertainty of the next observation. Using equations (5) and (6), the distribution after the next observation is specified by $N(\mu_1, \sigma_1^2)$; the distribution of its mean μ_1 is given by equations (8) and (9).

Based on the criterion on passability, if $W_{robot} < \mu_1 - 3\sigma_1$, then the space is passable; if $W_{robot} > \mu_1 + 3\sigma_1$, then the space is impassable; otherwise, the passability is unknown. Since the variance σ_1^2 of the distribution after the observation is constant, only the mean μ_1 affects the passability of the space. Thus, from the knowledge of the distribution of μ_1 (equations (8) and (9)), we can calculate, by the following equations, the three probabilities as:

$$
\begin{aligned}
P_\bigcirc &= \int_{W_{robot}+3\sigma_1}^{\infty} \frac{1}{\sqrt{2\pi\sigma_{\mu_1}^2}} e^{-(\mu_1-\mu_0)^2/2\sigma_{\mu_1}^2} d\mu_1, \\
P_\triangle &= \int_{W_{robot}-3\sigma_1}^{W_{robot}+3\sigma_1} \frac{1}{\sqrt{2\pi\sigma_{\mu_1}^2}} e^{-(\mu_1-\mu_0)^2/2\sigma_{\mu_1}^2} d\mu_1, \qquad (10) \\
P_\times &= \int_{-\infty}^{W_{robot}-3\sigma_1} \frac{1}{\sqrt{2\pi\sigma_{\mu_1}^2}} e^{-(\mu_1-\mu_0)^2/2\sigma_{\mu_1}^2} d\mu_1.
\end{aligned}
$$

These values correspond to integrations of the three parts shown in Fig. 11. We would like to stress that we can calculate the above three probabilities without knowing the actual observation result x_{obs}.
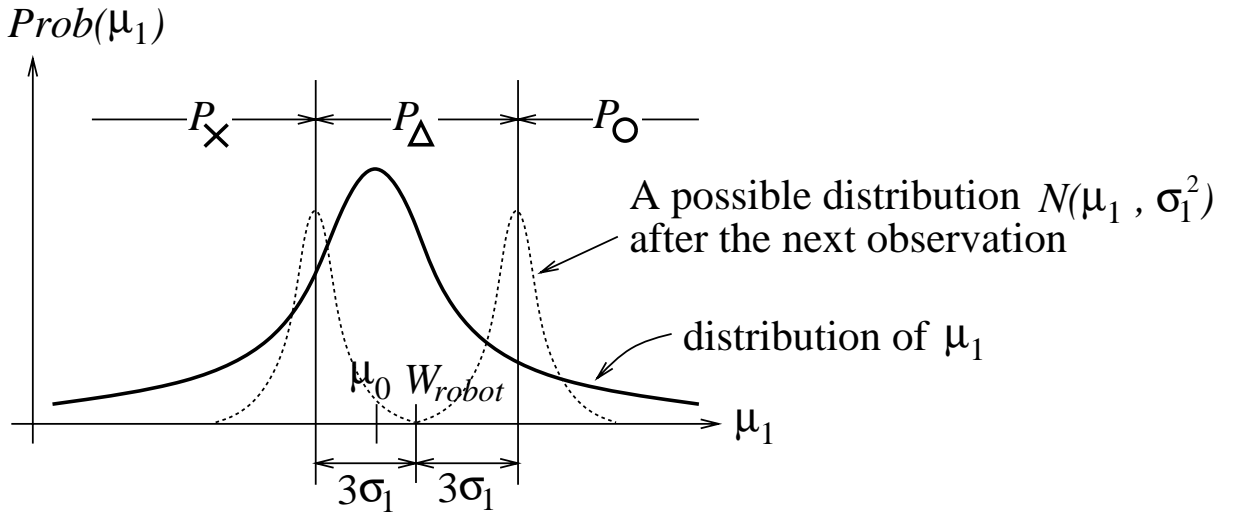
Figure 11: Calculation of three probabilities.

5 Calculating Lower Bound using Uncertainty Model of Visual Information

We use the branch-and-bound method with best-bound search to obtain the optimal solution efficiently, as described in Section 2.3. The branch-and-bound requires methods of calculating

the lower bound of each alternative for pruning. This section describes a method to calculate the lower bound using the uncertainty model of visual information.

5.1   Assumption of Perfect Sensor Information

Let $\boldsymbol{I}_u$ be information including uncertainty to be obtained by the next observation $\boldsymbol{O}$, and $\boldsymbol{I}_p$ be information to be obtained by assuming that $\boldsymbol{O}$ can provide information without uncertainty. The cost of a solution s_p based on $\boldsymbol{I}_p$ is less than or equal to that of a solution s_u based on $\boldsymbol{I}_u$. Therefore, s_p gives the lower bound of the cost of possible solutions. We call the cost of s_p the lower bound under the *assumption of perfect sensor information*.

In order to employ this, it is necessary to know what *perfect sensor information* is. If a property (e.g., the position of a segment) is to be sensed, perfect sensor information means that the variance of the distribution of the property is zero. Such information is, however, useless because the probability of obtaining each possibility of the perfect information is the obtained distribution itself.

If the possible situation is classified into several situations according to the values of properties, and if the cost can be calculated for each situation, the assumption of perfect sensor information provides useful information. The classification of the passability of a space is exactly such a case. Let us consider again the situation depicted in Fig. 1. Suppose the robot has obtained a probability distribution of the width of the space between objects. After the next observation, the robot classifies the situation into one the three cases as shown in Fig. 4. The probabilities ($P_\bigcirc$, $P_\times$ and $P_\triangle$) for the three cases are given by Equation (10). Let $P_\bigcirc^p$, $P_\times^p$ and $P_\triangle^p$ be the three corresponding probabilities under the assumption of perfect sensor information. These probabilities are obtained by letting observation uncertainty σ_{obs}^2 be zero in Equations (5), (6), and (10) as follows:

$$
\begin{aligned}
P_\bigcirc^p &= \int_{W_{robot}}^\infty \frac{1}{\sqrt{2\pi\sigma_0^2}} e^{-(\mu_1-\mu_0)^2/2\sigma_0^2} dw_1, \\
P_\triangle^p &= 0, \\
P_\times^p &= \int_{-\infty}^{W_{robot}} \frac{1}{\sqrt{2\pi\sigma_0^2}} e^{-(\mu_1-\mu_0)^2/2\sigma_0^2} dw_1.
\end{aligned}
\tag{11}
$$

Note that, under the assumption of perfect sensor information, the passability of the space is *perfectly* determined without knowing the actual observation result x_{obs}.

5.2   Calculating Lower Bounds

By applying the assumption of perfect sensor information to the current situation, a set of fixed situations with probabilities is obtained. Then, the lower bound $Cost_{lb}$ is obtained as the expectation of the total cost as follows:

$$
Cost_{lb} = C_{vision} + P_\bigcirc^p Cost_\bigcirc + P_\times^p Cost_\times,
\tag{12}
$$

where C_{vision} is the cost of one observation and $Cost_\bigcirc$ and $Cost_\times$ are the costs from the current position to the destination for the passable and the impassable case, respectively.

Using the uncertainty model of vision, a better lower bound can be computed for each candidate of the next observation point. Once an observation point $\boldsymbol{x}$ and a target of observation are chosen, the uncertainty σ_{obs}^2 is determined and thereby the probabilities ($P_\bigcirc$, $P_\times$ and $P_\triangle$) in

Equation (10) are calculated. In the case where the space is either passable or impassable, costs can be calculated. In the case where the passability is unknown, the lower bound is obtained by applying the assumption of perfect sensor information recursively. The better lower bound $Cost'_{lb}$ is calculated by

$$
\begin{aligned}
Cost'_{lb} &= C_{motion}(\boldsymbol{x}_{curr}, \boldsymbol{x}) + C_{vision} + P_{\bigcirc} Cost'_{\bigcirc} + P_{\times} Cost'_{\times} \\
&+ P_{\triangle}(C_{vision} + P_{\bigcirc}^{p'} Cost'_{\bigcirc} + P_{\times}^{p'} Cost'_{\times}),
\end{aligned}
\tag{13}
$$

where $\boldsymbol{x}_{curr}$ is the current position, $P_{\bigcirc}^{p'}$ and $P_{\times}^{p'}$ are the probabilities under the assumption obtained by an observation at $\boldsymbol{x}$, $Cost'_{\bigcirc}$ and $Cost'_{\times}$ are the cost from $\boldsymbol{x}$ to the destination for the passable and the impassable case, respectively (see Fig. 12).

Figure 12: Calculation of the lower bound $Cost'_{lb}$. Two dots for $\boldsymbol{x}$ is identical in actual. For the case that the passability is unknown at $\boldsymbol{x}$, the space is supposed to be observed again at the same place.

Since the uncertainty of the width of a space is represented by a normal distribution, the two values $P_{\triangle}P_{\bigcirc}^{p'}$ and $P_{\triangle}P_{\times}^{p'}$ are approximated by $P_{\bigcirc}^{p} - P_{\bigcirc}$ and $P_{\times}^{p} - P_{\times}$, respectively (see Appendix A). Thus, Equation (13) is approximated by

$$
Cost'_{lb} = C_{motion}(\boldsymbol{x}_{curr}, \boldsymbol{x}) + (1 + P_{\triangle})C_{vision} + P_{\bigcirc}^{p} Cost'_{\bigcirc} + P_{\times}^{p} Cost'_{\times}.
\tag{14}
$$

Since the value of $Cost'_{lb}$ depends on $\boldsymbol{x}$, the minimum value provides the lower bound at the current position. If there is only one space to be observed, the computational cost for obtaining the best $Cost'_{lb}$ is $\mathcal{O}(mn)$, where m and n are the numbers of observation points and observation conditions, respectively.

For example, Fig. 13 shows the lower bounds, which are calculated with Equation (14), for possible next observation points in front of the obstacles in Fig. 1. If the lower bound of a point is higher than the cost of the incumbent (the best feasible solution among those which have been acquired so far), the point can be eliminated from the candidates.
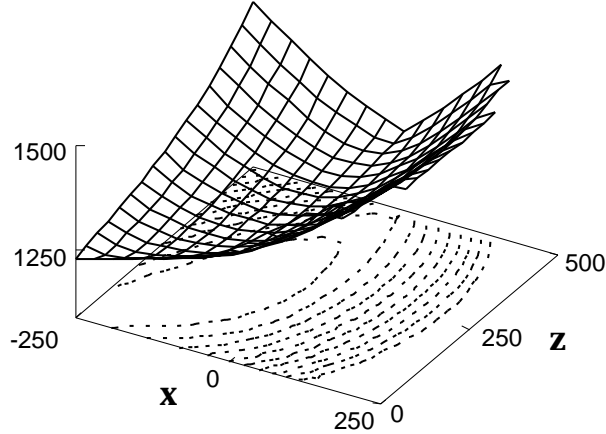
Figure 13: Lower bound of the cost for each observation point which is less than the incumbent value (the cost of the detour in this case). A robot is at $(-250, 0)$; the observed features of the obstacles are at $(-40, 500)$ and $(40, 500)$.

If there are multiple spaces to be observed in the environment, the lower bound is obtained by recursively applying the assumption of perfect sensor information to the spaces in turn. In this case, the lower bound is calculated for each triplet of the observation position, the observation condition and the space to be observed.

6   Simulation

This section first describes what should be done before implementing the proposed method, then presents simulation results on typical planning problems.

6.1   Problem

Simulation has been performed for typical problems. Fig. 14 shows a situation where a robot is surrounded by walls and gates. The cost from each gate to the goal point is given. Only the widths of the gates are uncertain, and the robot measures them by stereo vision. Based on the initial information obtained by observing each gate once at the initial position, a robot searches for observation points inside the walls. The cost is evaluated in terms of the distance to move, by assuming that the speed of the robot is constant, and that the time for one observation is constant and can be converted into an equivalent distance.

6.2   Implementation Issues

In order to solve the problem by search in a discrete space, several operations are necessary in advance: (1) observation points are limited only to grid points on the working environment of
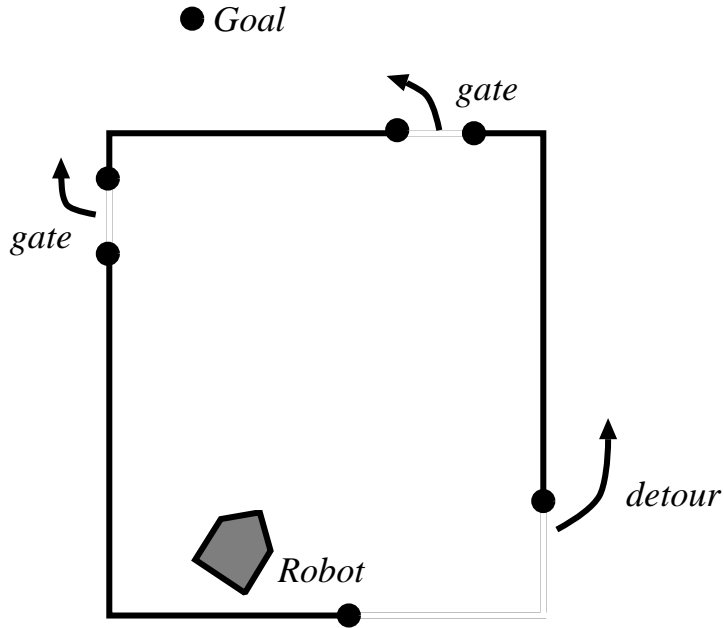
Figure 14: Simulation problem.

the robot; (2) if the passability of a space is unknown after an observation, the mean of the width of the space varies continuously from $W_{robot} - 3\sigma_1$ to $W_{robot} + 3\sigma_1$ as shown in Fig. 11. Each possible mean corresponds to a branch at an OR node (see Fig. 3). For such a case, we divide the range of the width into a predetermined number of discrete values, and continues further search for each value; (3) if the probability that the passability is unknown, which is given by Equation (10), is less than a certain threshold for a branch, the branch is not expanded further and is given the initial incumbent (see Section 2.4).

6.3   Results

Fig. 15 shows the planning results for the case where there is one gate to observe. The goal position is located above the left-upper corner of the wall. Solid lines indicate paths from the initial position to the next observation point. Dotted lines indicate possible paths from the next observation point. Branches with squares indicate planned observation points, and arrows indicate observation directions. Numbers attached to each path indicate the probability of taking the path. Of course, we cannot predict which path the robot actually takes because actual behaviors depend on further observation results.

In Figs. 15(a)-(c), if the gate is narrow, the next observation point is selected such that the cost of taking the detour is low. On the other hand, if the gate is broad, the next observation point is near to the gate. In Fig. 15(d), the gate is so broad that the robot decides to take the gate at the initial position.

Fig. 16 shows the simulation result for the case that there are two gates to observe. If $Gate_B$ is broader than $Gate_A$ as shown in Fig. 16(b), the next observation point is near to $Gate_B$ and the passability of only $Gate_B$ is decided by this observation. For the case that $Gate_B$ is impassable, a further plan including observations of only $Gate_A$ is generated by a recursive search.

(a) GateA is narrow.

(b) GateA is narrower.

(c) GateA is broad.

(d) GateA is broad enough.
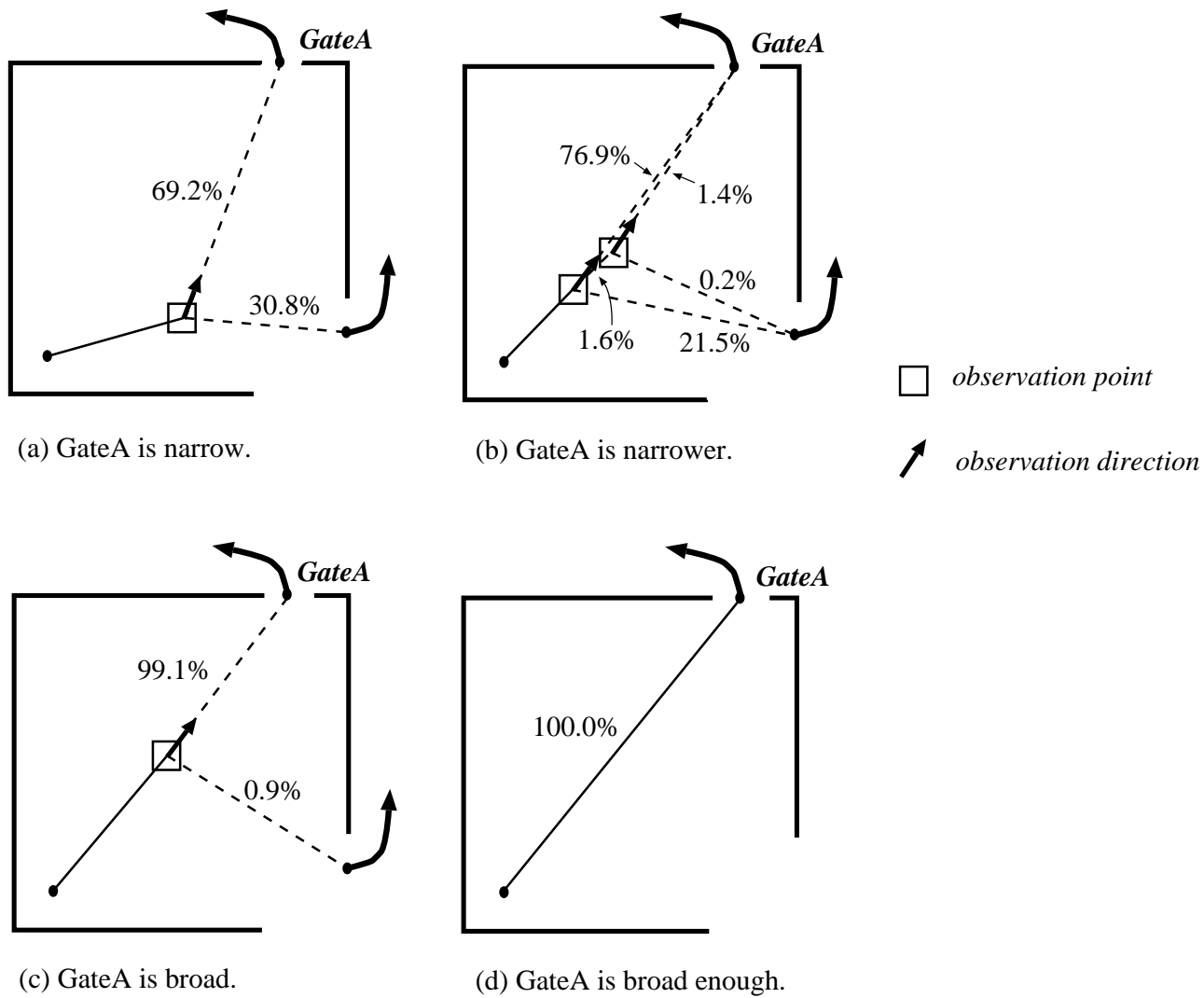
Figure 15: Simulation results (1): one gate to observe.

(a) Both gates have the same width.   (b) GateB is broader than GateA.
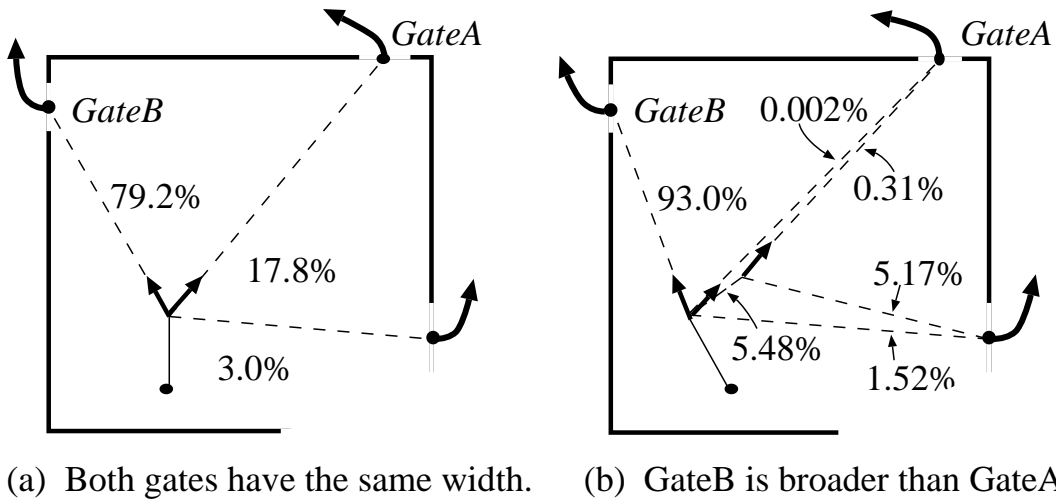
Figure 16: Simulation results (2): two gates to observe.

In order to evaluate our method, we compared it with the *adaptive behavior*, which chooses, among the following two behaviors, the one with less expected cost:

- *minimum-uncertainty behavior*: the robot always move to the point where the uncertainty of visual information is minimum. In this problem, the minimum-uncertainty point is the gate.

- *detour behavior*: the robot always takes the detour regardless of the passability of the gate.

This *adaptive behavior* is similar to the strategy employed in (Hu and Brady 1994).

Fig. 17 shows the comparison result for the problem shown in Fig. 15. We compared the two behaviors for several initial gate widths. The horizontal axis indicates the probability that the gate is passable, which is calculated from the gate width and the uncertainty of the initial observation. The vertical axis in the figure indicate the difference of an expected total cost and the lower bound of the total cost which is given by Equation (12). This result shows effectiveness of our method.

7 Experiments

7.1 Verification of Uncertainty Model

In the experiments, we first verified the uncertainty model, in which the width of a space is approximated with a normal distribution as described in Section 3.3. Fig. 18 shows the scene used for the examination; the width of the space composed of a blackboard and a cabinet was set to about 90 [cm]. We took about a hundred stereo data from the same observation point. Fig. 19 shows the histogram of the calculated space widths. The distribution of the observed data shows that the approximation with the normal distribution is reasonable.
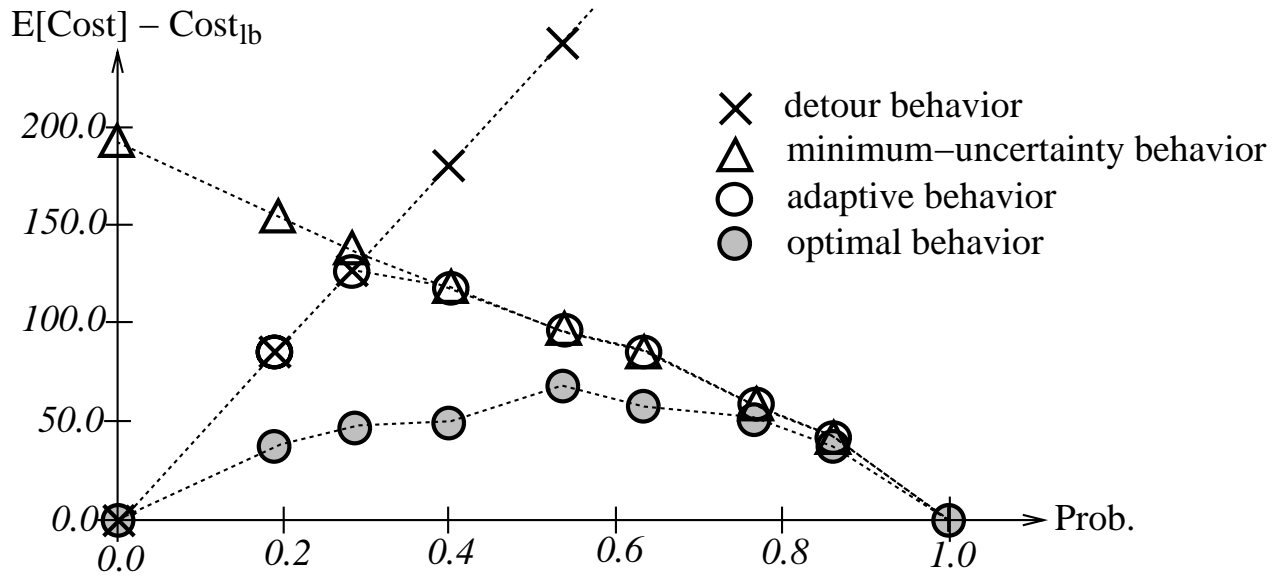
Figure 17: Comparison of the two behaviors. The horizontal axis (*Prob.*) indicates the probability that the gate is passable. The vertical axis indicates the difference between an expected total cost and the lower bound of the total cost calculated using Equation (12).

Figure 18: A scene used for examining the uncertainty model.
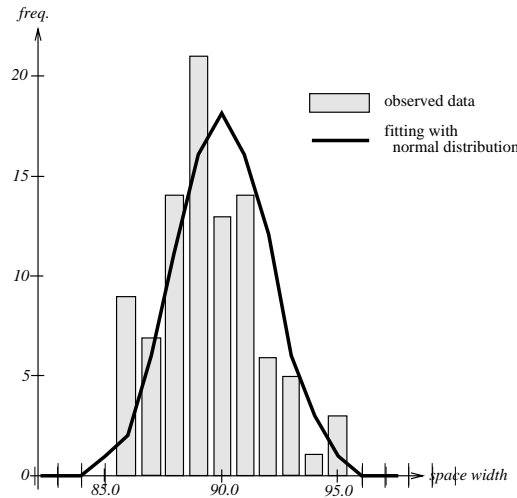
Figure 19: Histogram of the observed space widths and fitted normal distribution. The mean and the variance of the distribution are 90.1 [cm] and 4.42 [cm^2], respectively. Using these values, a discrete normal distribution is calculated, as indicated in the figure.

7.2 Planning Results for Real Problems

We applied the proposed method to an actual planning problem. Fig. 20 shows the experimental environment. A robot is going to the given destination. If the robot takes the shorter route to the destination, it has to pass the narrow space composed of a blackboard on the left side and a cabinet on the right. If the space is too narrow to pass, the robot takes a detour through the hallway. We will show below several results on this planning problem.

(a) Experimental setup.
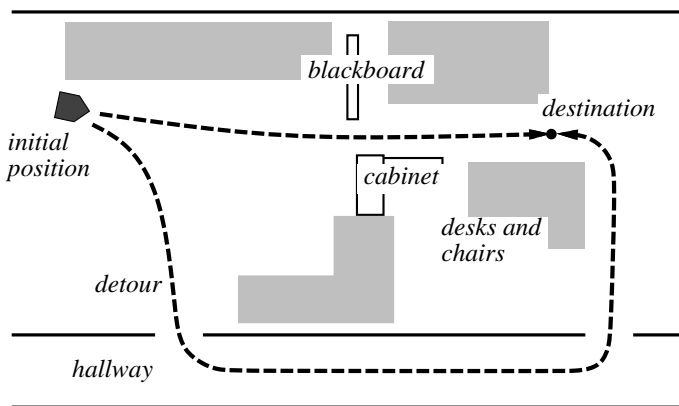
(b) Top view of the environment.

Figure 20: Experimental environment.

Fig. 21 shows a pair of stereo images taken at the initial position. Fig. 22 shows a set of vertical segments extracted from the left image, which are superimposed on the original image. The 3D position of these segments were calculated using our stereo method. In order to obtain the position of the blackboard and the cabinet, the 3D segments above the ground plane were first projected onto the floor, thereby obtaining a set of 2D points. By referring to

23

the approximate position of the objects given to the robot in advance, the segments shown in Fig. 23 were selected which belonged to the blackboard and the cabinet.

Figure 21: A pair of stereo images taken at the initial position.

Figure 22: Extracted segments in the left image.
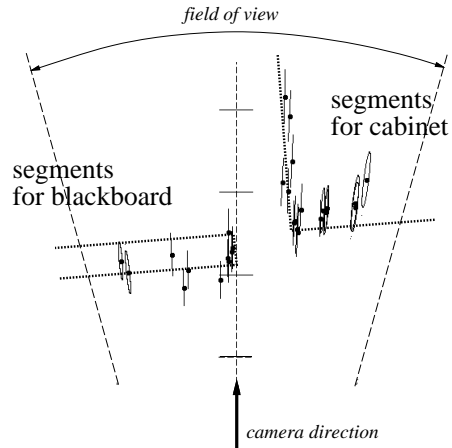
Figure 23: Obtained segments of the objects. Segments are extracted which are considered to belong to the blackboard or to the cabinet. The positional uncertainty of each segment is indicated by an ellipse as well as the mean position of the segment.

From these projected points, we selected the nearest pair of segments in terms of the Mahalanobis distance, one from the blackboard's segments and the other from the cabinet's. This pair was used to calculate the mean μ_d and the standard deviation σ_d of the probability distribution of the width of the space.

We added the margin W_{margin} to the actual width W_{robot} of the robot; if $\mu_d + 3\sigma_d$ $(\mu_d - 3\sigma_d)$ is smaller (larger) than $W_{robot} + W_{margin}$, the space is determined to be passable (impassable). In our experiment, W_{robot} is 64 $[cm]$ and W_{margin} was set to 15 $[cm]$.

As the initial estimate of the space width, we obtained $\mu_d = 80.77$ $[cm]$ and $\sigma_d = 1.953$ $[cm]$; the probability of the space being passable was calculated as 0.83. Based on these values, the plan shown in Fig. 24 was generated. Then, the robot proceeded to the first observation point, took another pair of stereo images shown in Fig. 25, and calculated the width of the space

between the objects. By integrating the two sets of data, we obtained the distribution with $\mu_d = 79.46$ [cm] and $\sigma_d = 0.092$ [cm]. From the integrated data, the robot determined the space was passable and passed through it towards the destination.
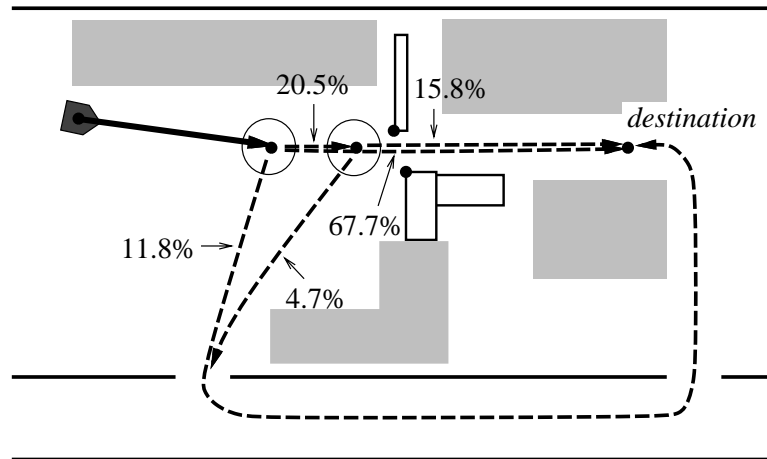
Figure 24: A generated plan for the data shown in Fig. 21. Circles indicate planned observation points. The solid arrow indicate the path to the next observation point. Dotted arrows indicate possible paths after the next observation. The probability of taking each path is also indicated in the figure.

Figure 25: A pair of stereo images taken at the planned next observation point.

Fig. 26 shows the stereo images taken at the initial position for another experiment, in which the space was set to be narrower than in the first experiment. From the initial data, the probability distribution of the space was calculated as $\mu_d = 77.97$ [cm] and $\sigma_d = 1.814$ [cm], from which the probability of the space being passable was estimated as 0.26. Based on these values, the plan shown in Fig. 27 was generated. At the planned next observation point, the robot took data shown in Fig. 28. By integrating the two sets of data, we obtained the distribution with $\mu_d = 78.3$ [cm] and $\sigma_d = 0.580$ [cm]. This time the passability of the space was still undecided, and the probability that the space was passable was estimated as 0.10. The robot made a plan from there using the newest information, and eventually decided to take the detour through the hallway.

Figure 26: A pair of stereo images for another experiment.
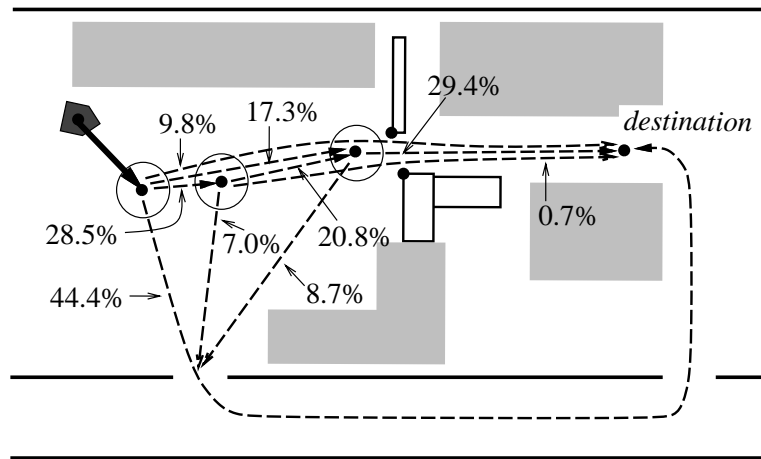
Figure 27: A generated plan for the data shown in Fig. 26. Circles indicate planned observation points. The solid arrow indicate the path to the next observation point. Dotted arrows indicate possible paths after the next observation. The probability of taking each path is also indicated in the figure.

Figure 28: A pair of stereo images taken at the planned next observation point in the second experiment.

8 Conclusion

This paper has formulated a vision-motion planning for a mobile robot under uncertainty of visual observations. By considering both the cost of motion and that of vision, the proposed method generates a globally optimal plan. An efficient pruning method is developed which is based on the lower bound of the total cost calculated under the assumption of perfect sensor information. Experimental results as well as simulation results demonstrated the feasibility of our approach. The proposed method can be applied to the robot which uses sensors other than vision as long as the error in sensor data is represented by a probabilistic model.

In spite of the efficient pruning, our current solution still requires too much computation to be used in real-time application. In the future work, we will take the following two approaches. One is to develop an approximation method that can be executed in real-time by extensively using domain-specific heuristics for pruning. The other approach is to develop a planning method which minimizes the expectation of the total cost of planning and execution. This method is based on knowledge of relationship between planning time and plan quality (Dean and Boddy 1988).

We have developed a method of modeling obstacles and free spaces from the stereo data with uncertainty (Miura and Shirai 1994). The modeling method generates a topological structure of possible routes and enumerates critical (narrow) regions whose passability should be examined. These information is enough for the proposed planning method to be applied to an unknown environment. We are now planning to conduct experiments using both the planning method and the environment modeling method.

References

Allen, P. K. et al. 1991. Automated Tracking and Grasping of a Moving Object with a Robotic Hand-Eye System. CUCS-034-91. Department of Computer Science, Columbia University.

Ayache, N. and Faugeras, O. D. 1989. Maintaining Representations of the Environment of a Mobile Robot. *IEEE Trans. on Robotics and Automation*, RA-5(6):804–819.

Berger, J. O. 1985. *Statistical Decision Theory and Bayesian Analysis*. Springer-Verlag, second edition.

Cameron, A. and H. Durrant-Whyte. 1990. A Bayesian Approach to Optimal Sensor Placement. *Int. J. of Robotics Res.*, 9:70–88.

Dean, T. and Boddy, M. 1988. An Analysis of Time-Dependent Planning. *Proc. The Seventh National Conf. on Artificial Intelligence*, pp. 49–54.

Dean, T., Basye, T., and Lejter, S. 1990. Planning and Active Perception. *Proc. 1990 DARPA Workshop on Innovative Approaches to Planning, Scheduling, and Control*, pp. 271–276.

Feldman, J. A. and Sproull, R. F. 1977. Decision Theory and Artificial Intelligence II: The Hungry Monkey. *Cognitive Science*, 1:158–192.

Fisz, M. 1963. *Probability Theory and Mathematical Statistics*. Wiley.

Hager, G. D. 1990. *Task-Directed Sensor Fusion and Planning: A Computational Approach.* Kluwer Academic Publishers.

Hu, H. and Brady, M. 1994. A Bayesian Approach to Real-Time Obstacle Avoidance for a Mobile Robot. *Autonomous Robots*, 1(1):69–92.

Hutchinson, S. A. and Kak, A. C. 1989. Planning Sensing Strategies in a Robot Work Cell with Multi-Sensor Capabilities. *IEEE Trans. on Robotics and Automation*, RA-5(6):765–783.

Ibaraki, T. 1987. Enumerative Approaches to Combinatorial Optimization. *Annals of Operations Res.*, 10 and 11.

Kriegman, D. J., Triendl, E., and Binford, T.O. 1989. Stereo Vision and Navigation in Buildings for Mobile Robots. *IEEE Trans. on Robotics and Automation*, RA-5(6):792–803.

Matthies, L. and Shafer, S. A. 1987. Error Modeling in Stereo Navigation. *IEEE J. of Robotics and Automation*, RA-3(3):239–248.

Medioni, G. and Nevatia, R. 1985. Segment-Based Stereo Matching. *Computer Vision, Graphics, Image Processing*, 31:2–18.

Miura, J. and Shirai, Y. 1992. Vision-Motion Planning with Uncertainty. *Proc. 1992 IEEE Int. Conf. on Robotics and Automation*, pp. 1772–1777.

Miura, J. and Shirai, Y. 1993. An Uncertainty Model of Stereo Vision and Its Application to Vision-Motion Planning of Robot. *Proc. the Thirteenth Int. Joint Conf. on Artificial Intelligence*, pp. 1618–1623.

Miura, J. and Shirai, Y. 1994. Modeling Obstacles and Free Spaces for a Mobile Robot using Stereo Vision with Uncertainty. *Proc. 1994 IEEE Int. Conf. on Robotics and Automation*, pp. 3368–3373.

Zhang, H. 1992. Optimal Sensor Placement. *Proceedings of 1992 IEEE Int. Conf. on Robotics and Automation*, pp. 1825–1830.

A   Calculation of $P_\triangle P_\bigcirc^{p'}$ and $P_\triangle P_\times^{p'}$

The value of $P_\triangle P_\bigcirc^{p'}$ is, referring to Fig. 11 and Equation (11), given by

$$
\begin{aligned}
P_\triangle P_\times^{p'} &= \int_{W_{robot}-3\sigma_1}^{W_{robot}+3\sigma_1} \frac{1}{\sqrt{2\pi\sigma_{\mu_1}^2}} e^{-(\mu_1-\mu_0)^2/2\sigma_{\mu_1}^2} \left(\int_{-\infty}^{W_{robot}} \frac{1}{\sqrt{2\pi\sigma_1^2}} e^{-(u-\mu_1)^2/2\sigma_1^2} du \right) d\mu_1 \\
&= \int_{-\infty}^{W_{robot}} \frac{1}{\sqrt{2\pi\sigma_0^2}} e^{-(u-\mu_0)^2/2\sigma_0^2} \left(\int_{W_{robot}-3\sigma_1}^{W_{robot}+3\sigma_1} \frac{1}{\sqrt{2\pi\sigma_A^2}} e^{-(\mu_1-\mu_A)^2/2\sigma_A^2} d\mu_1 \right) du \\
&\qquad \left(\text{where } \sigma_A^2 = \frac{\sigma_0^4\sigma_{obs}^2}{(\sigma_0^2+\sigma_{obs}^2)^2}, \ \mu_A = \frac{\sigma_{obs}^2\mu_0 + \sigma_0^2 u}{\sigma_0^2+\sigma_{obs}^2} \right) \\
&= \int_{-\infty}^{W_{robot}} \frac{1}{\sqrt{2\pi\sigma_0^2}} e^{-(u-\mu_0)^2/2\sigma_0^2} \left(1 - \int_{-\infty}^{W_{robot}-3\sigma_1} \frac{1}{\sqrt{2\pi\sigma_A^2}} e^{-(\mu_1-\mu_A)^2/2\sigma_A^2} d\mu_1 \right.
\end{aligned}
$$

$$-\int_{W_{robot}+3\sigma_1}^{\infty} \frac{1}{\sqrt{2\pi\sigma_A^2}} e^{-(\mu_1-\mu_A)^2/2\sigma_A^2} d\mu_1 \Bigg) du$$

$$= \int_{-\infty}^{W_{robot}} \frac{1}{\sqrt{2\pi\sigma_0^2}} e^{-(u-\mu_0)^2/2\sigma_0^2} du$$

$$- \int_{-\infty}^{W_{robot}-3\sigma_1} \frac{1}{\sqrt{2\pi\sigma_{\mu_1}}} e^{-(\mu_1-\mu_0)^2/2\sigma_{\mu_1}^2} \int_{-\infty}^{W_{robot}} \frac{1}{\sqrt{2\pi\sigma_1^2}} e^{-(u-\mu_1)^2/2\sigma_1^2} du d\mu_1$$

$$- \int_{W_{robot}+3\sigma_1}^{\infty} \frac{1}{\sqrt{2\pi\sigma_{\mu_1}}} e^{-(\mu_1-\mu_0)^2/2\sigma_{\mu_1}^2} \int_{-\infty}^{W_{robot}} \frac{1}{\sqrt{2\pi\sigma_1^2}} e^{-(u-\mu_1)^2/2\sigma_1^2} du d\mu_1.$$

In the second term, since the term

$$\int_{-\infty}^{W_{robot}} \frac{1}{\sqrt{2\pi\sigma_1^2}} e^{-(u-\mu_1)^2/2\sigma_1^2} du$$

is inside the integration of μ_1 from $-\infty$ to $W_{robot} - 3\sigma_1$, this term is the probability that the second observation result u satisfies $-\infty < u \le W_{robot}$ in case that the first fusion result μ_1 satisfies $-\infty < \mu_1 \le W_{robot} - 3\sigma_1$. This probability is almost one because the probability of acquiring u is $N(\mu_1, \sigma_1^2)$ and $\mu + 3\sigma_1 \le W_{robot}$. Similarly in the third term,

$$\int_{-\infty}^{W_{robot}} \frac{1}{\sqrt{2\pi\sigma_1^2}} e^{-(u-\mu_1)^2/2\sigma_1^2} du$$

is the probability that u satisfies $-\infty < u \le W_{robot}$ in case that μ satisfies $W_{robot} + 3\sigma_1 \le \mu < \infty$. This probability is almost zero because the probability of acquiring u is $N(\mu_1, \sigma_1^2)$ and $\mu_1 - 3\sigma_1 \ge W_{robot}$. Therefore, the value of $P_\triangle P_{\times}^{p'}$ is approximated by

$$P_\triangle P_{\times}^{p'} \approx \int_{-\infty}^{W_{robot}} \frac{1}{\sqrt{2\pi\sigma_0^2}} e^{-(u-\mu_0)^2/2\sigma_0^2} du - \int_{-\infty}^{W_{robot}-3\sigma_1} \frac{1}{\sqrt{2\pi\sigma_{\mu_1}^2}} e^{-(\mu_1-\mu_0)^2/2\sigma_{\mu_1}^2} d\mu_1$$

$$= P_{\times}^p - P_{\times}$$

Similarly, the following approximation also holds:

$$P_\triangle P_{\bigcirc}^{p'} \approx P_{\bigcirc}^p - P_{\bigcirc}.$$